ANNALS OF TRANSPLANTATION

ORIGINAL PAPER

e-ISSN 2329-0358
© Ann Transplant, 2026; 31: e952366
DOI: 10.12659/AOT.952366

Received: 2025.12.08
Accepted: 2026.03.27
Available online: 2026.04.16
Published: 2026.XX.XX

iTRAQ- and MRM-Based Proteomics Identify Early Injury Biomarkers for Primary Dysfunction After Liver Transplantation

Authors' Contribution:
Study Design A
Data Collection B
Statistical Analysis C
Data Interpretation D
Manuscript Preparation E
Literature Search F
Funds Collection G

ABCE 1,2 Xiaohong Lin*
ABCE 3 Wanzhen Cai*
ABCE 1 Xitao Hong*
BC 3 Ziming Ye
BC 1 Yuqi Dong
CD 1 Shuai Wang
ADFG 1 Xiaoshun He
CDE 4 Donghong Li
ADG 1 Weiqiang Ju
ADEFG 1 Maogen Chen

1 Organ Transplant Center, the First Affiliated Hospital, Sun Yat-sen University; Guangdong Provincial Key Laboratory of Organ Medicine, Guangzhou, Guangdong, PR China
2 Department of Breast and Thyroid Surgery, Eastern Hospital of the First Affiliated Hospital of Sun Yat-sen University, Guangzhou, Guangdong, PR China
3 Department of Critical Care Medicine, the First Affiliated Hospital, Sun Yat-sen University; Guangdong Clinical Research Center for Critical Care Medicine, Guangzhou, Guangdong, PR China
4 Department of Neurology, Third Affiliated Hospital, Sun Yat-sen University, Guangzhou, Guangdong, PR China

* Xiaohong Lin, Wanzhen Cai, and Xitao Hong contributed equally to this work

Corresponding Authors: Maogen Chen, e-mail: chenmg3@mail.sysu.edu.cn, Weiqiang Ju, e-mail: weiqiangju@163.com, Donghong Li, e-mail: lidh58@mail.sysu.edu.cn

Financial support: This work was supported by the National Natural Science Foundation of China (82470613) and the Guangdong Provincial Key Laboratory of Organ Medicine (2023B1212060020), China

Conflict of interest: None declared

Background: Primary nonfunction (PNF) is a severe complication following liver transplantation (LT), yet precise molecular biomarkers for early identification of patients at risk remain lacking, which can delay timely therapeutic intervention.

Material/Methods: Liver biopsies were collected from patients and classified into 4 groups: control, optimal graft (OG), early allograft dysfunction (EAD), and PNF. Samples were obtained at 3 time points: T0 (pre-cold perfusion), T1 (pre-reperfusion), and T2 (post-reperfusion). Isobaric tags for relative and absolute quantitation (iTRAQ) and multiple reaction monitoring (MRM) were used for proteomic analysis and biomarker verification.

Results: Baseline characteristics of the patients showed no significant differences between groups. A total of 6505 proteins were identified in human liver samples. There were 160 differentially expressed proteins (67 upregulated and 93 downregulated) found in the PNF group compared to the control, while 54 and 36 proteins were identified in the EAD and OG groups, respectively. Ten proteins were selected for MRM verification, confirming the significant upregulation of VWF and downregulation of PRDX1, HGD, THIO, 6PGD, and HPPD, consistent with the iTRAQ results.

Conclusions: PRDX1, HGD, THIO, 6PGD, HPPD, and VWF were identified as candidate proteins associated with PNF and ischemia-reperfusion injury (IRI) after LT. These findings are hypothesis-generating and require validation in larger, independent cohorts to determine their potential clinical value.

Keywords: Biomarkers • Ischemia-Reperfusion Injury • Liver Transplantation • Proteomics

Full-text PDF: https://www.annalsoftransplantation.com/abstract/index/idArt/952366

Indexed in: [Science Citation Index Expanded] [Index Medicus/MEDLINE] [Chemical Abstracts] [Scopus]

Introduction

Liver transplantation (LT) is the only effective treatment for end-stage liver disease. Liver grafts are classified into 3 categories based on liver function recovery: optimal graft function (OG), early allograft dysfunction (EAD), and primary nonfunction (PNF). The quality of liver allografts is closely linked to ischemia-reperfusion injury (IRI). Severe IRI can lead to EAD or PNF, both of which significantly affect patient and allograft survival [1-4].

PNF is a severe complication of LT, characterized by unexpected graft dysfunction, often requiring immediate retransplantation or resulting in patient death [5]. In Canada and France, the annual loss rate for transplanted organs can reach as high as 10% [6]. PNF is a multifactorial syndrome, with risk factors including high donor body mass index (BMI), moderate to severe steatosis, prolonged cold or warm ischemic times, and grafts from donation after circulatory death (DCD) [7]. Studies link cold ischemia times over 10 h and warm ischemia times exceeding 40 minutes with higher PNF incidence [8-10]. Additionally, DCD grafts are a significant risk factor for PNF [11]. Other donor-related factors, such as prolonged intensive care unit (ICU) stays (>5 days), hypernatremia, and diabetes, also increase PNF risk [12]. Given its complexity, no single factor or biomarker reliably predicts outcomes. Currently, the primary strategy to prevent PNF involves careful selection of donors and recipients based on known risk factors, including donor laboratory tests, clinical risk scores, organ appearance, and, in some cases, biopsies and perfusion parameters. However, these methods are limited and insufficient to fully prevent PNF [13]. The ideal biomarker for PNF should demonstrate high sensitivity for the early detection of graft injury, along with sufficient specificity to reliably distinguish PNF from other post-transplant complications that present with similar clinical features, such as acute rejection, biliary complications, or vascular insufficiency. This discriminative capacity is of critical importance, given that the therapeutic strategies are fundamentally different. For instance, PNF primarily results from severe IRI and often necessitates supportive care or retransplantation, whereas acute rejection requires immediate immunosuppressive intervention [14,15]. A biomarker that lacks specificity can result in diagnostic uncertainty, potentially delaying appropriate management or exposing patients to unnecessary and potentially ineffective treatments [16]. It is therefore vital to identify molecular signatures that uniquely reflect the pathophysiological processes underlying PNF, including mitochondrial dysfunction, microcirculatory disturbance, and hepatocyte necrosis, to clarify early differential diagnosis and inform accurate medicine strategies following LT. Advancements in technologies such as imaging, transcriptomics, genomics, proteomics, metabolomics, lipidomics, and organ perfusion have provided new insights into the mechanisms underlying IRI, inflammation, and graft rejection. These technologies offer the potential to identify biomarkers that could help predict PNF risk after LT and aid in the acceptance or rejection of suboptimal liver grafts. Such biomarker panels would likely need to account for multiple factors involved in the transplantation process.

Kornasiewicz et al applied a proteomic approach to identify protein phenotypes associated with PNF after LT, but without further validation [17]. Isobaric tags for relative and absolute quantitation (iTRAQ) is a powerful proteomic method that combines stable isotope labeling with tandem mass spectrometry for precise comparative quantification. Multiple reaction monitoring (MRM) is a targeted proteomic technique known for its high reproducibility and sensitivity in complex samples. Several studies have demonstrated the feasibility of using MRM-MS for quantitative proteomic analysis, offering multiplexed, precise, specific, and standardized quantification. Moreover, iTRAQ discovery followed by MRM verification has been used in biomarker quantification studies [18], but its application for predicting the quality of donor livers has been limited.

In this study, we used iTRAQ as a discovery tool, followed by MRM verification, to conduct a comparative proteomic analysis aimed at identifying key proteins indicative of potential hepatic injury in grafts at risk of PNF after LT. Our goal was to identify early biomarkers associated with PNF that can be measured after LT, providing insights for individualized clinical therapies to prevent PNF.

Material and Methods

Liver biopsy samples from 20 patients were used for iTRAQ and MRM validation. Clinical data were collected from 20 liver transplant recipients and donors, categorized into 4 groups: Control (n=5), OG (n=5), EAD (n=5), and PNF (n=5). In the Control group, normal liver biopsy samples were obtained from 5 optimal organ donors, with corresponding EAD and PNF recipients excluded (**Figure 1**).

Liver biopsies were collected at 3 time points during transplantation. For the Control group, samples were taken before cold perfusion during organ harvesting (designated as T0). Donor livers were preserved at 4°C in University of Wisconsin solution and transplanted after preservation. In the experimental groups, liver samples from 15 grafts were collected at 2 additional time points. The second biopsy, representing cold ischemia injury, was obtained before liver recirculation (T1). A third biopsy was taken after 2 h of liver reperfusion (T2). All liver tissues were immediately stored in liquid nitrogen.

Samples were collected between November 2015 and March 2017 at the First Affiliated Hospital of Sun Yat-sen University (FAH-SYSU), China. Written informed consent was obtained

Indexed in: [Science Citation Index Expanded] [Index Medicus/MEDLINE] [Chemical Abstracts] [Scopus]

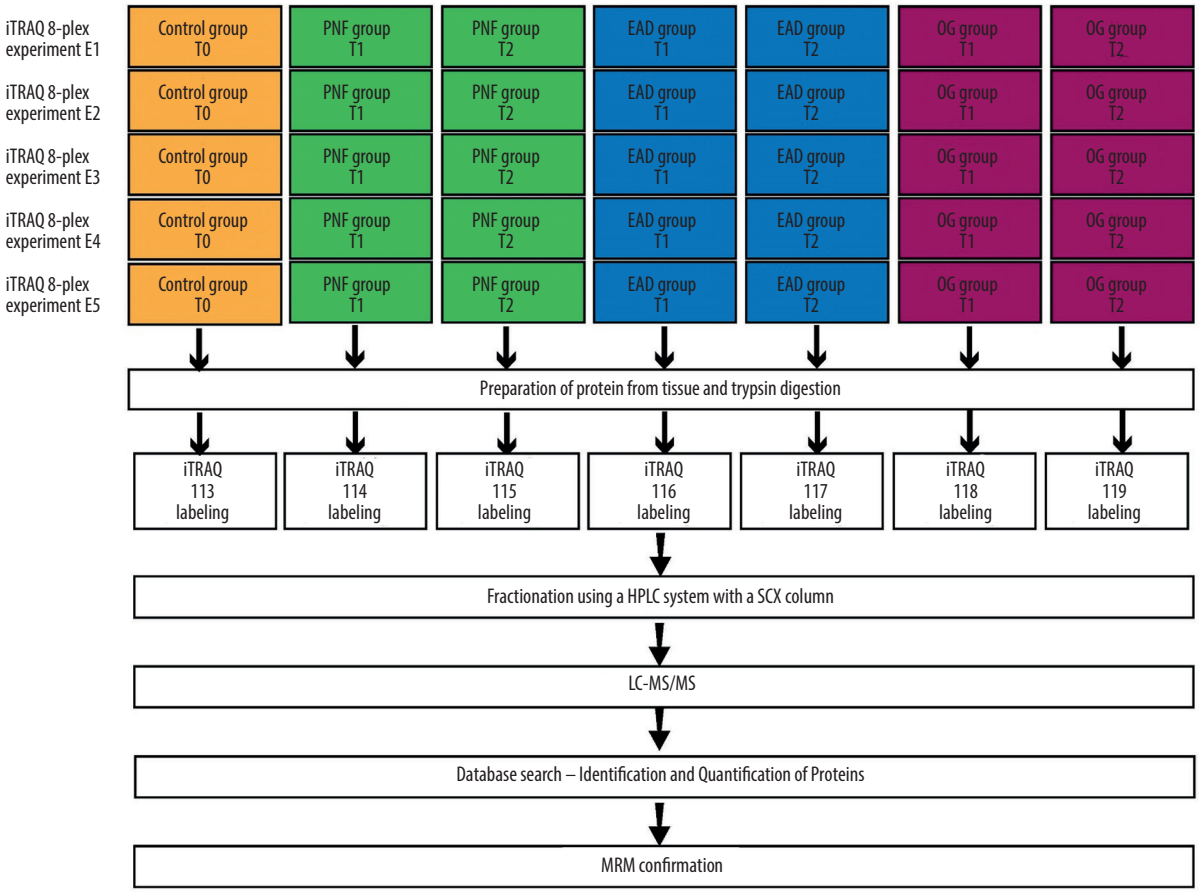

Figure 1. General proteomics workflow for patient sampling, iTRAQ labeling, and protein verification.

from all recipients, and the study adhered to the ethics guidelines of the 1975 Declaration of Helsinki. The study was approved by the Clinical Research Ethics Committee of FAH-SYSU (approval number: [2021] No. 117). No organs from executed prisoners were used. PNF was defined as AST or ALT >1500 IU/L in 2 consecutive tests within the first 72 h, leading to retransplantation or recipient death [19].

Protein Preparation and SDS-PAGE Electrophoresis

Proteins were extracted using lysis buffer (1 mM PMSF, 2 mM EDTA, 7 M urea, 2 M thiourea, 4% CHAPS, 40 mM Tris-HCl, pH 8.5). After 5 min, 10 mM DTT was added for reduction. The homogenized tissue was centrifuged at 25 000×g for 15 min at 4°C. The supernatant was further reduced with DTT, incubated at 56°C for 1 h, and cysteine residues were blocked with 55 mM iodoacetamide (IAM) on ice for 45 min. Proteins were precipitated with chilled acetone, incubated for 2 h, and centrifuged. The pellet was dissolved in 0.5 M TEAB, sonicated, and the supernatant was collected for analysis. Protein concentrations were determined by Bradford assay. SDS-PAGE was performed to assess protein integrity. Thirty micrograms of protein from each sample were loaded onto 10% gels, stained with Coomassie Brilliant Blue, and selected for trypsin digestion and LC-MS/MS analysis based on clear, defined bands.

Quantitative iTRAQ Analysis

One hundred micrograms of protein from each sample group were digested with 2.5 µg trypsin (Promega, USA) at a 40: 1 protein-to-trypsin ratio at 37°C for 4 h, followed by an additional 8-h incubation for complete digestion. The resulting peptides were desalted using a Strata X C18 column (Phenomenex, USA) and dried by vacuum centrifugation. Peptides were dissolved in 0.5 M TEAB and labeled with 8-plex iTRAQ reagents (Applied Biosystems, USA) according to the manufacturer's protocol. The PNF2, PNF1, EAD2, EAD1, OG2, OG1, and Control groups were labeled with 7 distinct iTRAQ tags. Each reagent was dissolved in 24 µL isopropanol, and peptides were incubated with the reagent at room temperature for 2 h before being dried via vacuum centrifugation.

Indexed in: [Science Citation Index Expanded] [Index Medicus/MEDLINE] [Chemical Abstracts] [Scopus]

Strong Cation Exchange (SCX) chromatography was performed using an LC-20AB HPLC pump system (Shimadzu, Japan). The labeled peptides were combined, reconstituted in 2 mL buffer (5% acetonitrile [ACN], pH 9.8), and loaded onto a 4.6×250 mm Gemini C18 column (Thermo Fisher Scientific, USA). Peptides were eluted at 1 mL/min with the following gradient: 0-10 min: 5% buffer (95% ACN, pH 9.8); 10-50 min 5-35% buffer; 50-51 min: 35-90% buffer. Fractions were collected every minute and monitored at 214 nm absorbance, resulting in 20 fractions. These fractions were desalted and vacuum dried for further analysis.

Each fraction was dissolved in 2% ACN, 0.1% formic acid (FA) and centrifuged at 20 000×g for 10 min. The supernatant was loaded onto a C18 trap column (75 µm inner diameter, Phenomenex, USA) in an LC-20AD nano HPLC system (Shimadzu, Japan). Peptides were separated at a flow rate of 300 nL/min using the following gradient: 0-8 min: 5% buffer (98% ACN, 0.1% FA); 8-43 min: 5-35% buffer; 43-48 min: 35-60% buffer; 48-50 min: 60-80% buffer; 50-55 min: 80% buffer; 55-56 min: return to 5% buffer.

The separated peptides were analyzed with a Q-Exactive tandem mass spectrometer (Thermo Fisher Scientific, USA) via nanospray ionization. Data acquisition was performed in data-dependent acquisition (DDA) mode, with full MS scans obtained using the Orbitrap mass analyzer across a 350-1600 m/z range at a resolution of 70 000. The 20 most intense multiply charged precursor ions (intensity >10 000) were selected for fragmentation via higher-energy collision-induced dissociation (HCD). Tandem mass spectra were acquired in the Orbitrap at a resolution of 17 500 at 100 m/z. A 15-s dynamic exclusion was applied to prevent repeated sequencing of the same precursor ions.

Data Processing and Protein Identification

All primary mass spectrometry data were converted to MGF (Mascot Generic Format) files for downstream analysis. Protein identification was performed using the Mascot search engine (Matrix Science, London, UK) integrated within the IQuant software. To ensure high-confidence identification and significantly reduce false positives, the Mascot Percolator algorithm was used. A strict false discovery rate (FDR) threshold of ≤1% was enforced at both the peptide-spectrum match (PSM) and protein levels using the Picked protein FDR strategy.

Differential Expression Analysis

For the iTRAQ-based discovery phase, proteins were considered candidate differentially expressed proteins if they met the following criteria: a fold change ≥1.2, an $P<0.05$ (t test), and reproducibility in at least 3 independent experiments. To maximize the discovery potential from highly heterogeneous clinical liver samples and to minimize Type II errors, strict multiple testing corrections were intentionally not applied to the P values during this exploratory screening phase. This liberal threshold was chosen to capture a broad range of potentially relevant proteins for hypothesis generation, with an explicit design in which a rigorous false-positive control would be strictly enforced in the downstream targeted MRM validation phase.

Functional Annotation and Enrichment Analysis

For functional annotation, protein sequences were analyzed using Blast2GO by comparing them with the non-redundant protein (NR) database from NCBI. The KEGG (Kyoto Encyclopedia of Genes and Genomes) database and COG (Clusters of Orthologous Groups of Proteins) database were used to classify proteins based on their biological pathways, functional roles, and orthologous relationships. Enrichment analysis was conducted to identify key metabolic and regulatory pathways associated with the differentially expressed proteins. For each GO term and KEGG pathway, enrichment significance was assessed using the hypergeometric test (or Fisher's exact test). Consistent with the exploratory, hypothesis-generating nature of the discovery phase, terms and pathways with an $P<0.05$ were considered significantly enriched. Multiple testing corrections were not applied here to avoid masking broader biological trends at this preliminary stage.

MRM Validation of Differentially Expressed Proteins Identified by iTRAQ

A total of 10 differentially expressed proteins were selected for MRM validation. Samples were digested with trypsin as described previously and spiked with 50 fmol β-galactosidase for label-free data normalization. MRM analysis was performed on a QTRAP 5500 mass spectrometer (SCIEX, USA) coupled with an LC-20AD nano HPLC system (Shimadzu, Japan). The mobile phase consisted of Solvent A (0.1% aqueous formic acid) and Solvent B (98% acetonitrile, 0.1% formic acid). Peptide separation was carried out on a C18 column (0.075×150 mm, 3.6 µm particle size) at 300 nL/min with the following gradient: 0-38 min: 5-30% solvent B; 38-42 min: 30-80% solvent B; and 42-50 min: 80% solvent B (maintenance). The QTRAP 5500 was operated with a spray voltage of 2400 V, nebulizer gas pressure of 23 psi, and a dwell time of 10 ms per transition. Multiple MRM transitions were monitored at unit resolution in both Q1 and Q3 quadrupoles to maximize specificity.

Raw data were processed using Skyline software, applying the iRT (indexed retention time) strategy to compare peptide spectra against a pre-established spectral library. All transitions for each peptide were used for quantification unless interference from the sample matrix was observed. The MRM signal was

Indexed in: [Science Citation Index Expanded] [Index Medicus/MEDLINE] [Chemical Abstracts] [Scopus]

defined by the detection of all transitions from the endogenous peptide coeluting with the stable isotope-labeled peptide, confirmed by equivalent retention times and consistent relative areas of light and heavy transitions. Precision was evaluated by calculating the coefficient of variation (CV) as the standard deviation divided by the mean.

For the MRM validation of pre-selected candidate proteins, we applied a stringent statistical approach using MS stats with a linear mixed-effects model. An FDR correction was applied using the Benjamini–Hochberg method with a cutoff of 0.05. Proteins were considered significantly differentially expressed if the FDR <0.05 and fold change ≥1.5. The more stringent fold-change threshold was chosen to prioritize robust candidates with larger-magnitude changes and to reduce false positives.

Statistical Analysis

Statistical analyses were performed using SPSS version 22.0 and GraphPad Prism version 8.0. Continuous variables were expressed as mean±standard error of the mean (SEM) or median with interquartile range (IQR), and categorical variables as frequencies and percentages. Normality was assessed using the Shapiro–Wilk test and Q-Q plots, and homogeneity of variances by Levene's test. For comparisons between 2 groups, the *t* test was used for normally distributed data with homogeneous variances; otherwise, the Mann–Whitney U test was applied. For multiple-group comparisons, one-way ANOVA or the Kruskal-Wallis test was used, depending on whether parametric assumptions were met. Categorical variables were compared using the chi-square test or Fisher's exact test. All tests were 2-tailed, and $P<0.05$ was considered statistically significant.

Results

Demographic and Clinical Characteristics of Recipients and Donors

Twenty liver transplant recipients were selected for proteomics analysis, with demographic and clinical data summarized in **Table 1**. The primary diagnoses included liver failure (most common), hepatocellular carcinoma, and 1 case of primary biliary cirrhosis. Preoperative mean Model for End-Stage Liver Disease (MELD) scores were 26.8±12.8 for the PNF group, 14.8±7.7 for the EAD group, 16.6±13.1 for the OG group, and 17.4±7.1 for the Control group, with no significant differences observed between groups ($F=0.685$, $P>0.05$), indicating similar baseline liver function.

Clinical characteristics such as cold ischemia time (CIT) and warm ischemia time (WIT) are presented in **Table 1**. Statistical analysis showed no significant differences in these parameters ($P>0.05$), suggesting a consistent surgical environment. Seventy-five percent of the donors were male, with traumatic brain injury (60%) and cardiovascular events (30%) being the leading causes of donor death.

Exploration of Proteomics in Liver Transplantation and Unveiling Key Proteins in IRI

iTRAQ-based quantitative proteomics was performed to analyze proteomic changes in donor livers before and after reperfusion. A total of 1 719 726 spectra were obtained, leading to the identification of 75 665 unique peptides and 6505 proteins using Mascot software (**Figure 2**). Of these, 6048 proteins were annotated via Gene Ontology (GO), allowing functional categorization.

Among the identified proteins, 5406 (including 33 unique proteins) were classified under biological processes, with enriched GO terms including single-organism processes, metabolic processes, cellular processes, and biological regulation. Additionally, 5417 proteins (including 91 unique) were associated with molecular functions, primarily catalytic activity and binding. Cellular component annotation identified 5783 proteins associated with cellular structures such as cells, organelles, membranes, and cell parts. A total of 4892 proteins were mapped to all 3 GO categories (biological process, molecular function, and cellular component), providing a comprehensive overview of protein functions (**Figure 3A**).

KEGG pathway enrichment analysis revealed that 4756 proteins (78.64% of identified proteins) were mapped to 324 pathways (**Figure 3B**). The most-enriched pathways included metabolic pathways (15.11%), endocytosis (3.6%), PI3K-Akt signaling (3.05%), phagosomes (2.64%), and protein processing in the endoplasmic reticulum (2.43%). Key regulatory pathways identified included PI3K-Akt (182 proteins), MAPK (107 proteins), Ras (98 proteins), mTOR (84 proteins), and apoptosis (82 proteins), all critical in LT. Comparative proteomics analysis revealed 579 differentially expressed proteins with significant upregulation or downregulation following liver reperfusion (**Figure 3C**).

Potential Mechanisms of Metabolic Reprogramming and Inflammatory Response in Differentially Expressed Proteins of Liver Transplantation

To identify proteins associated with IRI and to evaluate their stage-specific relevance, we compared the proteomic profiles of the OG2, EAD2, and PNF2 groups against the Control group at T2. Differentially abundant proteins (DAPs) were identified using a fold-change threshold >1.2 and $P<0.05$. A total of 220 DAPs were identified in the PNF2 vs Control comparison, comprising 91 upregulated and 129 downregulated proteins

Indexed in: [Science Citation Index Expanded] [Index Medicus/MEDLINE] [Chemical Abstracts] [Scopus]

Table 1. Clinical characteristics of donors, recipients and transplantation procedures.

Characteristics	Control (n=5)	OG (n=5)	EAD (n=5)	PNF (n=5)	*P* value
Donor					
Sex, M/F (% male)	4/1 (80%)	4/1 (80%)	3/2 (60%)	4/1 (80%)	1.000
Age, median (median and range)	37.8 (13-64)	22.2 (13-46)	35.8 (19-49)	34.4 (24-43)	0.342
BMI (mean±SD)	21.2±2.74	20.92±1.73	23.4±1.68	23.8±2.56	0.986
ICU stay, days (median and range)	3.2 (1-7)	3.2 (2-7)	2.7 (1-6)	3.3 (3-7)	0.918
Steatosis macrovesicular >10% (%)	0%	0%	20%	20%	1.000
HBsAg (+) (%)	20%	0%	20%	0%	1.000
CIT, min (median and range)	471 (289-651)	389 (282-540)	487 (390-582)	539 (360-714)	0.062
Donation type, DBD/DCD (% of DBD)	5/0 (100%)	4/1 (80%)	4/1 (80%)	3/2 (60%)	0.472
Recipient					
Sex M/F (% of male)	4/1 (80%)	5/0 (100%)	5/0 (100%)	4/1 (80%)	0.472
Age, median (median and range)	50.8 (38-67)	53.2 (46-61)	47.6 (34-55)	51.6 (29-67)	0.682
BMI (mean±SD)	23.7±3.38	24.2±3.70	26.2±1.25	20.7±2.21	0.056
Lab MELD score at transplantation (mean±SD)	17.4±7.1	16.6±13.1	14.8±7.7	26.8±12.8	0.573
Child-Pugh points, A/B/C	3/2/0	2/2/1	2/3/0	2/1/2	0.576
WIT, min (median and range)	NA	6 (6)	3 (3)	10 (8-12)	NA
Outcome					
Graft survival at 1 year (%)	100%	100%	100%	0%	**<0.001**
Recipient survival at 1 year (%)	100%	100%	100%	0%	**<0.001**
In-house/30-day mortality (%)	0%	0%	0%	100%	**<0.001**
ICU stay, days (median and range)	4 (2-10)	4 (2-7)	4 (2-7)	6 (3-9)	0.745

P<0.05 means a significant difference.

(**Figure 4A**). Notably, among these, 160 proteins including 67 upregulated and 93 downregulated proteins were uniquely altered in the PNF2 group and were not significantly changed in the EAD2 or OG2 groups at the same post-reperfusion time point. This observation suggests that these 160 proteins possess specificity for the PNF outcome rather than merely reflecting a generalized response to the transplant procedure or reperfusion itself.

The top 20 enriched pathways for each group (PNF2, EAD2, OG2 vs Control) were analyzed and summarized in **Table 2**, with overlap visualized in a Venn diagram (**Figure 4B**). Two pathways – metabolic pathways and Glyoxylate and Dicarboxylate Metabolism – were co-enriched across multiple groups. Eleven pathways were specifically enriched in the PNF group, including Glycolysis/Gluconeogenesis, Fatty Acid Degradation, Tyrosine Metabolism, and others, suggesting significant metabolic reprogramming in PNF following ischemia-reperfusion injury. Complete enrichment results, including gene ratios, fold enrichment values, and *P* values for all significant pathways in each group, are provided in **Table 3**.

GO enrichment analysis showed that 91 proteins were involved in biological processes such as Glycolysis, Citrate Cycle, Tyrosine

Indexed in: [Science Citation Index Expanded] [Index Medicus/MEDLINE] [Chemical Abstracts] [Scopus]

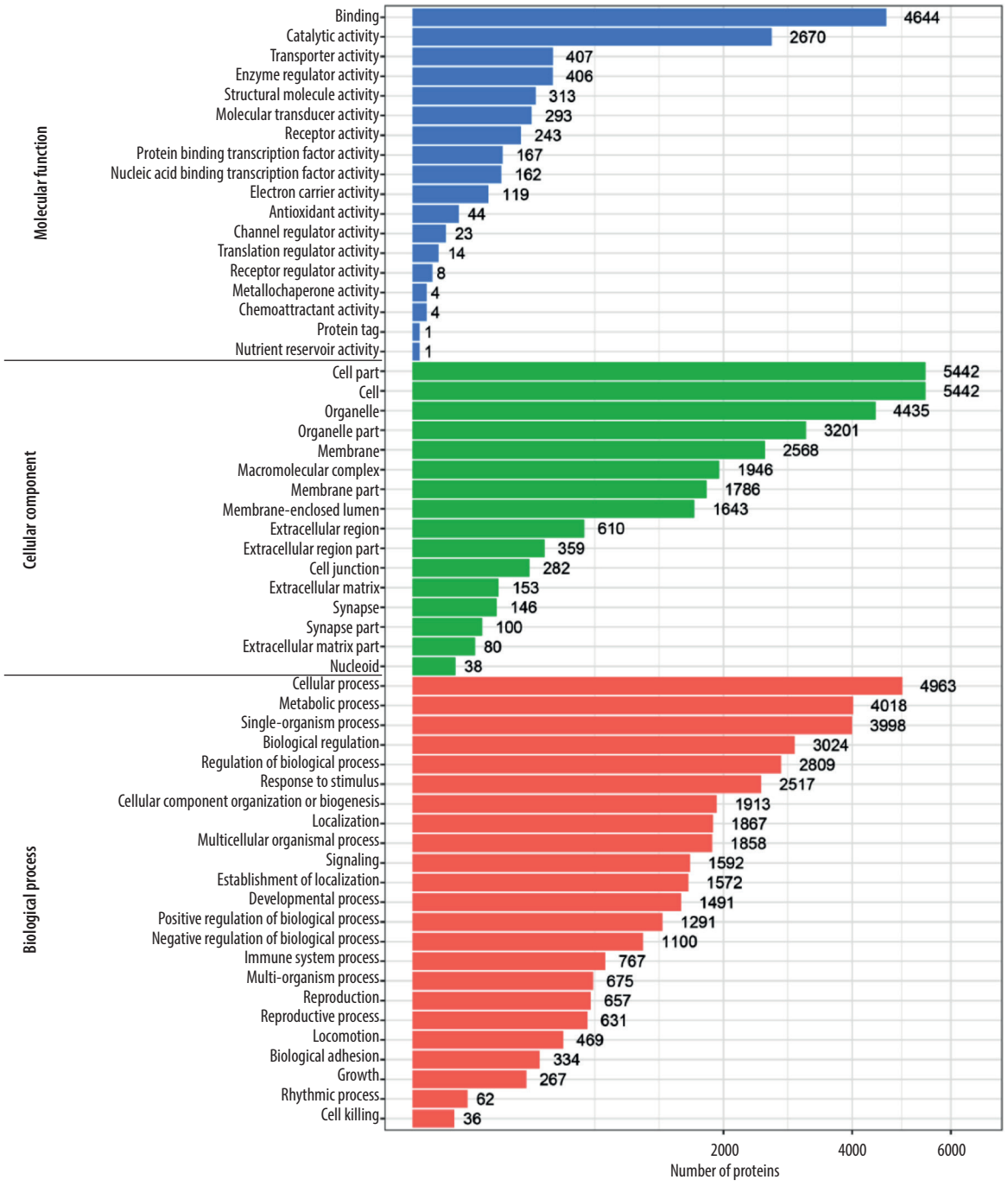

Figure 2. The differential proteins in human liver tissues during transplantation were analyzed using proteomics data. The proteins were functionally annotated with Gene Ontology (GO) for biological process, molecular function, and cellular component.

Indexed in: [Science Citation Index Expanded] [Index Medicus/MEDLINE] [Chemical Abstracts] [Scopus]

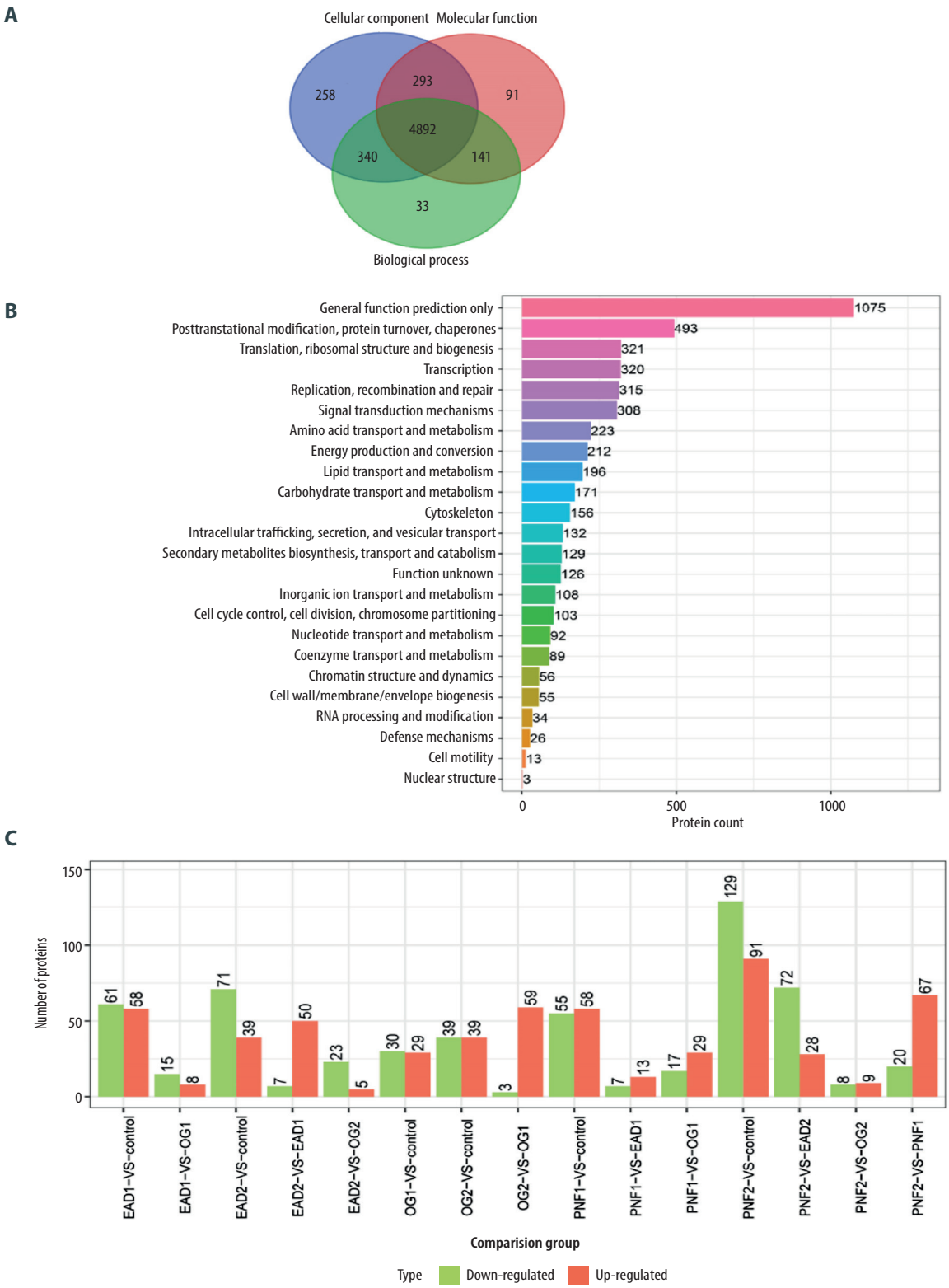

Figure 3. Venn diagram of the annotation of the proteins for the 3 processes. (**A**) The proteins were divided by COG functional classification. (**B**) The differentially expressed proteins between the groups are shown (n=5). (**C**) Red column: upregulated proteins, and green column: downregulated proteins (n=5).

Indexed in: [Science Citation Index Expanded] [Index Medicus/MEDLINE] [Chemical Abstracts] [Scopus]

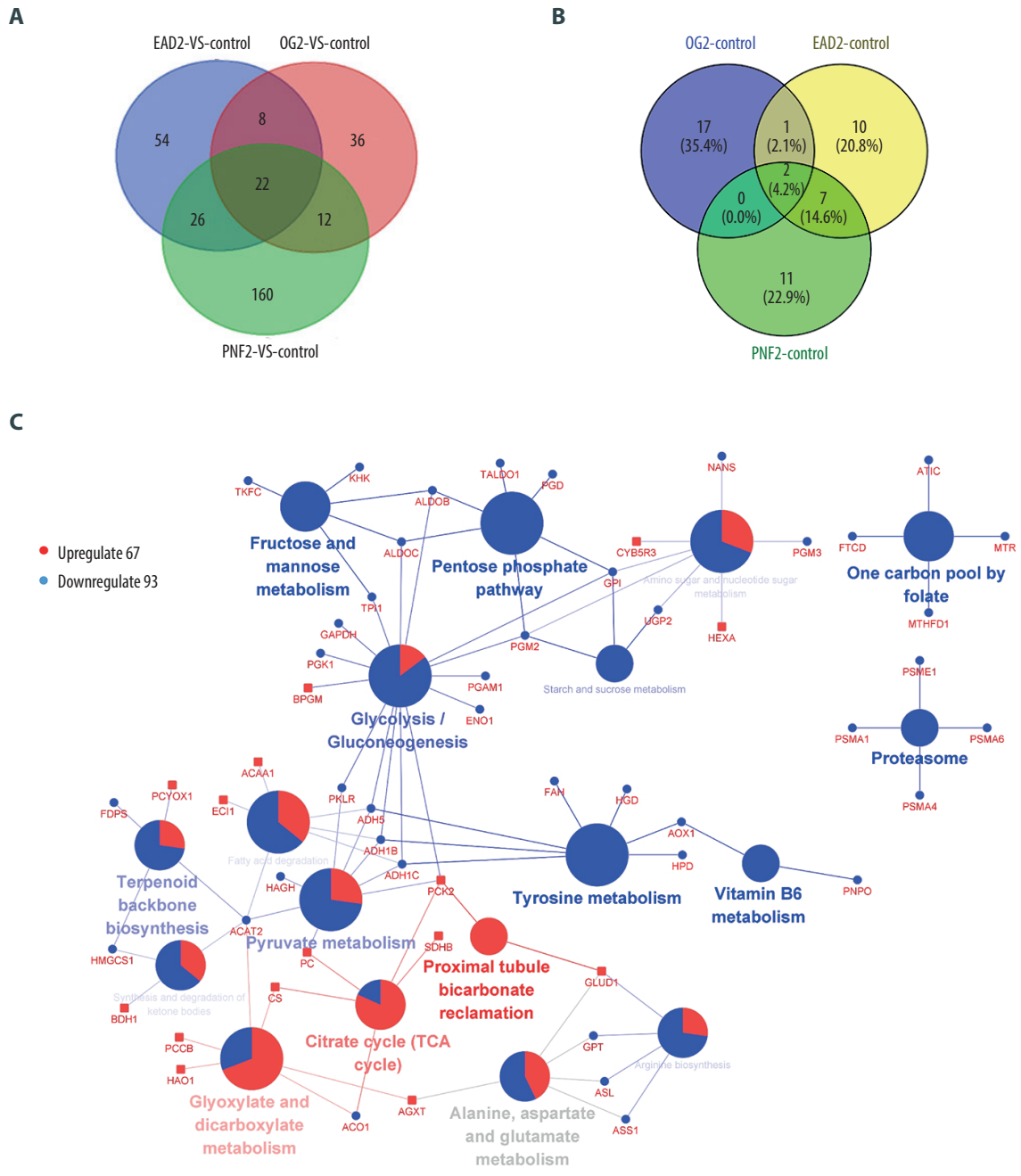

Figure 4. Comparison of the proteins identified in the control and tissue groups after reperfusion groups, which might play important roles in IRI pathogenesis. (**A**) Venn diagram of the differentially expressed proteins between the PNF2 (n=5), EAD2 (n=5), OG2 (n=5), and Control liver tissue (n=5). (**B**) Venn diagram showing the top 20 KEGG pathways and co-enriched pathways. (**C**) The cluster analysis of the common proteins that were differentially expressed in PNF2 vs Control group (n=5).

Indexed in: [Science Citation Index Expanded] [Index Medicus/MEDLINE] [Chemical Abstracts] [Scopus]

Table 2. Top 20 pathways in KEGG pathway analysis of the liver proteome datasets after reperfusion.

Rank	OG group	EAD group	PNF group
1	Histidine metabolism	Biosynthesis of amino acids	Metabolic pathways
2	Measles	Complement and coagulation cascades	Carbon metabolism
3	Amoebiasis	Metabolic pathways	Biosynthesis of amino acids
4	Transcriptional misregulation in cancer	Nitrogen metabolism	Glycolysis/gluconeogenesis
5	Staphylococcus aureus infection	Carbon metabolism	Glyoxylate and dicarboxylate metabolism
6	Fat digestion and absorption	Glyoxylate and dicarboxylate metabolism	Fatty acid degradation
7	Proximal tubule bicarbonate reclamation	Citrate cycle (TCA cycle)	Arginine biosynthesis
8	Proteasome	Proximal tubule bicarbonate reclamation	Tyrosine metabolism
9	Fc gamma R-mediated phagocytosis	Arginine biosynthesis	Citrate cycle (TCA cycle)
10	IL-17 signaling pathway	Pathogenic Escherichia coli infection	Amino sugar and nucleotide sugar metabolism
11	Systemic lupus erythematosus	2-Oxocarboxylic acid metabolism	2-Oxocarboxylic acid metabolism
12	Mineral absorption	Glutathione metabolism	Pentose phosphate pathway
13	Ascorbate and aldarate metabolism	Fluid shear stress and atherosclerosis	Fructose and mannose metabolism
14	Metabolic pathways	Butanoate metabolism	Retinol metabolism
15	Pentose and glucuronate interconversions	beta-Alanine metabolism	Ribosome
16	PPAR signaling pathway	Glycosaminoglycan biosynthesis - heparan sulfate/heparin	Glycine, serine and threonine metabolism
17	Neuroactive ligand-receptor interaction	Vitamin B6 metabolism	Peroxisome
18	Insect hormone biosynthesis	Glycosaminoglycan biosynthesis – chondroitin sulfate/dermatan sulfate	Complement and coagulation cascades
19	Glycerolipid metabolism	Protein processing in endoplasmic reticulum	Butanoate metabolism
20	Glyoxylate and dicarboxylate metabolism	Cardiac muscle contraction	One carbon pool by folate

Indexed in: [Science Citation Index Expanded] [Index Medicus/MEDLINE] [Chemical Abstracts] [Scopus]

Table 3. Enrichment analysis results for OG, EAD, and PNF groups.

Rank	OG group	Gene ratio	Fold enrichment	*P* value
1	Histidine metabolism	3.9%	8.79	0.00231
2	Measles	6.49%	3.75	0.00392
3	Amoebiasis	6.49%	3.71	0.00413
4	Transcriptional misregulation in cancer	6.49%	3.39	0.00611
5	Staphylococcus aureus infection	5.19%	3.47	0.0129
6	Fat digestion and absorption	2.6%	8.21	0.0154
7	Proximal tubule bicarbonate reclamation	2.6%	8.21	0.0154
8	Proteasome	3.9%	3.34	0.0175
9	Fc gamma R-mediated phagocytosis	5.19%	2.88	0.0226
10	IL-17 signaling pathway	3.9%	3.01	0.0235
11	Systemic lupus erythematosus	5.19%	2.86	0.0235
12	Mineral absorption	2.6%	3.50	0.0320
13	Ascorbate and aldarate metabolism	2.6%	3.50	0.0320
14	Metabolic pathways	23.38%	1.23	0.0354
15	Pentose and glucuronate interconversions	2.6%	2.46	0.0406
16	PPAR signaling pathway	3.9%	2.40	0.0417
17	Neuroactive ligand-receptor interaction	2.6%	2.20	0.0499
18	Insect hormone biosynthesis	1.3%	9.98	0.0628
19	Glycerolipid metabolism	2.6%	2.41	0.0634
20	Glyoxylate and dicarboxylate metabolism	2.6%	2.33	0.0669
Rank	**EAD group**	**Gene ratio**	**Fold enrichment**	***P* value**
1	Biosynthesis of amino acids	4.72%	4.03	0.00775
2	Complement and coagulation cascades	4.72%	3.57	0.0127
3	Metabolic pathways	23.58%	1.56	0.0134
4	Nitrogen metabolism	1.89%	10.25	0.0154
5	Carbon metabolism	5.66%	2.82	0.0193
6	Glyoxylate and dicarboxylate metabolism	2.83%	5.12	0.0201
7	Citrate cycle (TCA cycle)	2.83%	5.12	0.0201
8	Proximal tubule bicarbonate reclamation	1.89%	7.52	0.0281
9	Arginine biosynthesis	1.89%	6.27	0.0396
10	Pathogenic Escherichia coli infection	2.83%	3.93	0.0401
11	2-Oxocarboxylic acid metabolism	1.89%	5.93	0.0438

Indexed in: [Science Citation Index Expanded] [Index Medicus/MEDLINE] [Chemical Abstracts] [Scopus]

Table 3 continued. Enrichment analysis results for OG, EAD, and PNF groups.

Rank	EAD group	Gene ratio	Fold enrichment	*P* value
12	Glutathione metabolism	2.83%	3.76	0.0449
13	Fluid shear stress and atherosclerosis	3.77%	2.68	0.0613
14	Butanoate metabolism	1.89%	4.34	0.0769
15	beta-Alanine metabolism	1.89%	4.18	0.0821
16	Glycosaminoglycan biosynthesis – heparan sulfate/heparin	0.94%	11.28	0.0856
17	Vitamin B6 metabolism	0.94%	11.28	0.0856
18	Glycosaminoglycan biosynthesis – chondroitin sulfate/dermatan sulfate	0.94%	9.40	0.102
19	Protein processing in endoplasmic reticulum	4.72%	1.94	0.114
20	Cardiac muscle contraction	1.89%	3.32	0.121
Rank	**PNF group**	**Gene ratio**	**Fold enrichment**	***P* value**
1	Metabolic pathways	40.65%	2.69	<0.001
2	Carbon metabolism	12.62%	6.28	<0.001
3	Biosynthesis of amino acids	8.88%	7.58	<0.001
4	Glycolysis/gluconeogenesis	7.48%	7.33	<0.001
5	Glyoxylate and dicarboxylate metabolism	3.74%	6.77	<0.001
6	Fatty acid degradation	4.21%	5.85	<0.001
7	Arginine biosynthesis	2.80%	9.31	<0.001
8	Tyrosine metabolism	3.27%	6.52	<0.001
9	Citrate cycle (TCA cycle)	3.27%	5.92	<0.001
10	Amino sugar and nucleotide sugar metabolism	3.74%	4.56	<0.001
11	2-Oxocarboxylic acid metabolism	2.34%	7.35	<0.001
12	Pentose phosphate pathway	2.80%	5.78	<0.001
13	Fructose and mannose metabolism	2.80%	5.40	<0.001
14	Retinol metabolism	3.27%	4.55	<0.001
15	Ribosome	5.61%	2.75	0.00131
16	Glycine, serine and threonine metabolism	2.80%	4.79	0.00133
17	Peroxisome	4.21%	3.26	0.00159
18	Complement and coagulation cascades	4.21%	3.18	0.00191
19	Butanoate metabolism	2.34%	5.37	0.00200
20	One carbon pool by folate	1.87%	6.98	0.00207

P value <0.05 means a significant difference.

Indexed in: [Science Citation Index Expanded] [Index Medicus/MEDLINE] [Chemical Abstracts] [Scopus]

A

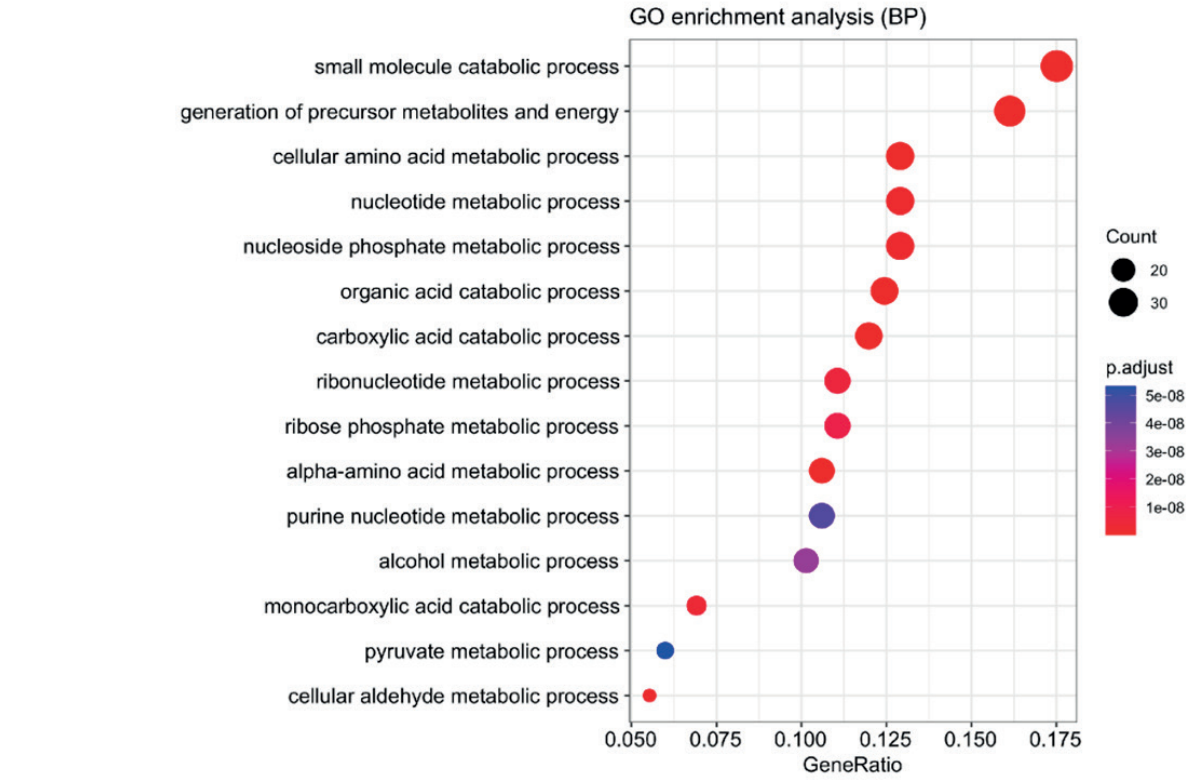

B

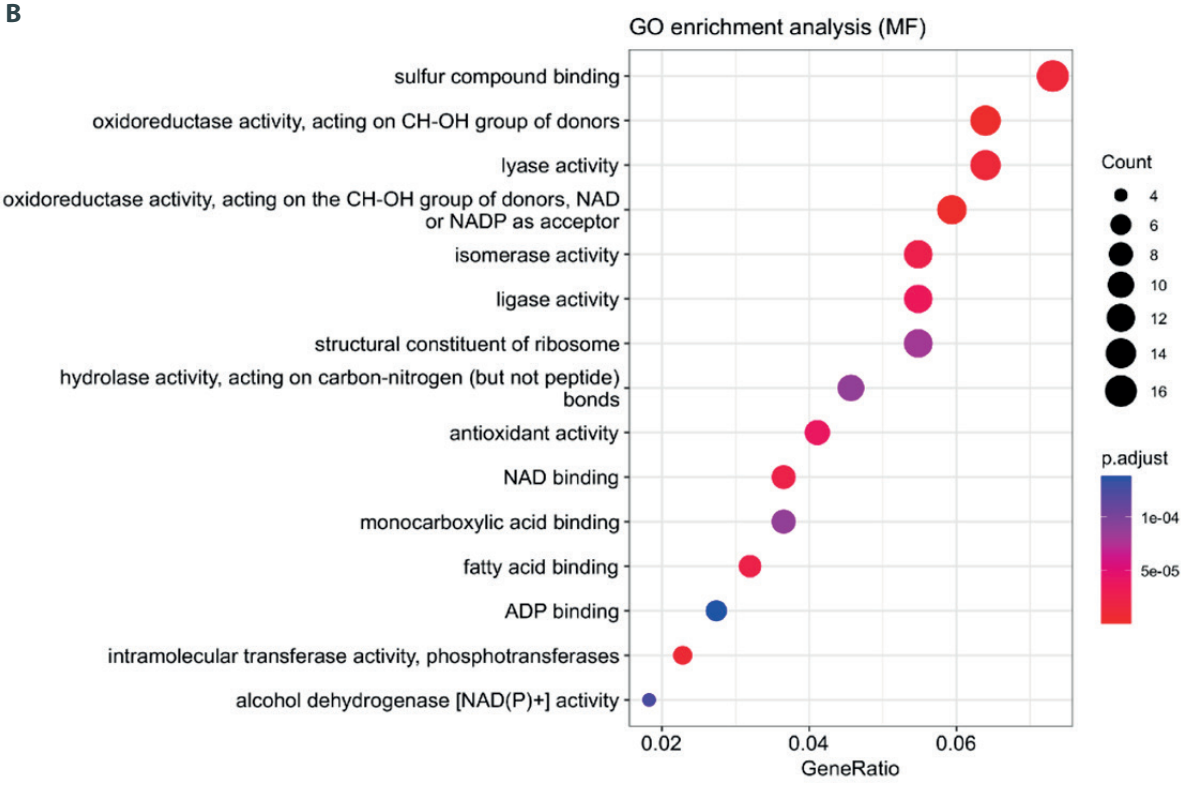

Indexed in: [Science Citation Index Expanded] [Index Medicus/MEDLINE] [Chemical Abstracts] [Scopus]

C

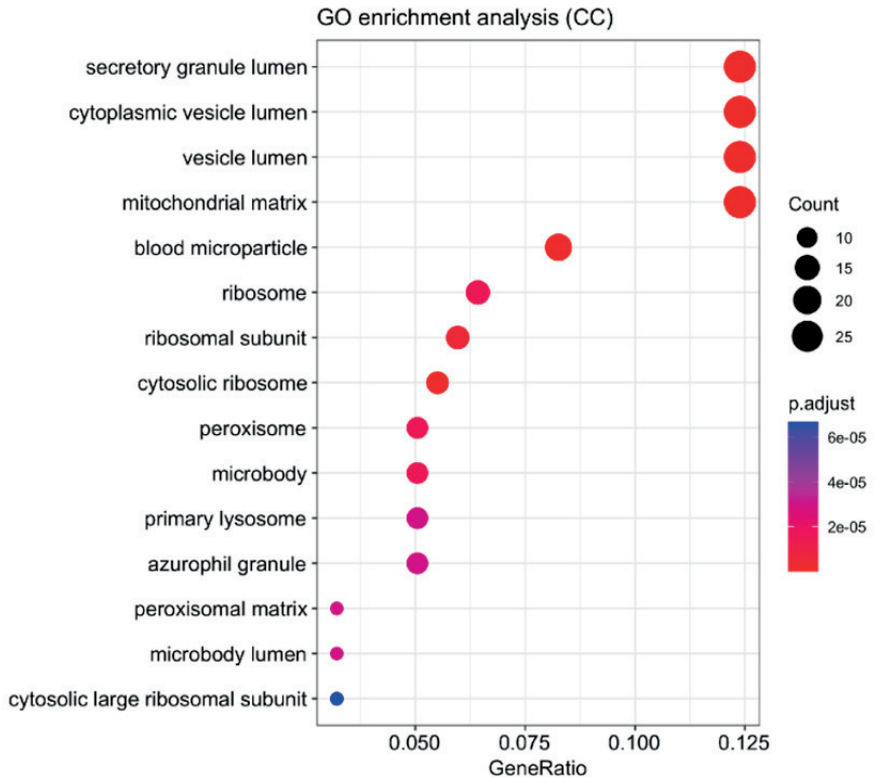

D

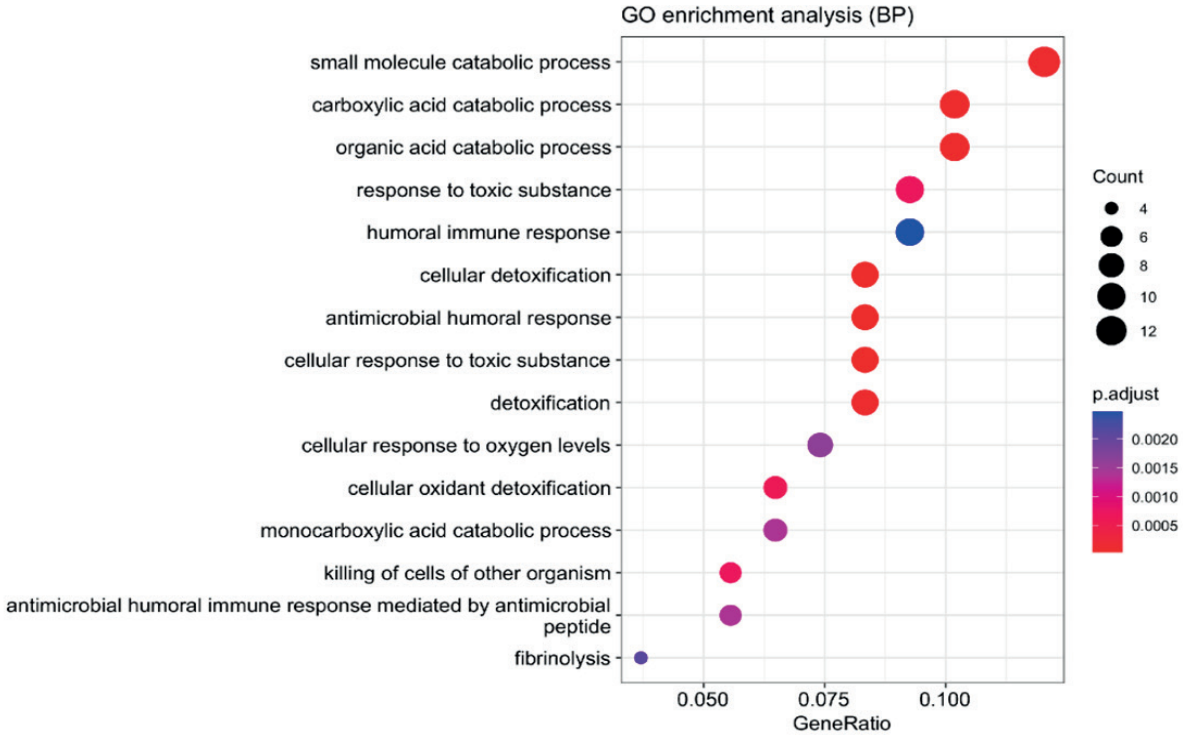

Indexed in: [Science Citation Index Expanded] [Index Medicus/MEDLINE] [Chemical Abstracts] [Scopus]

E

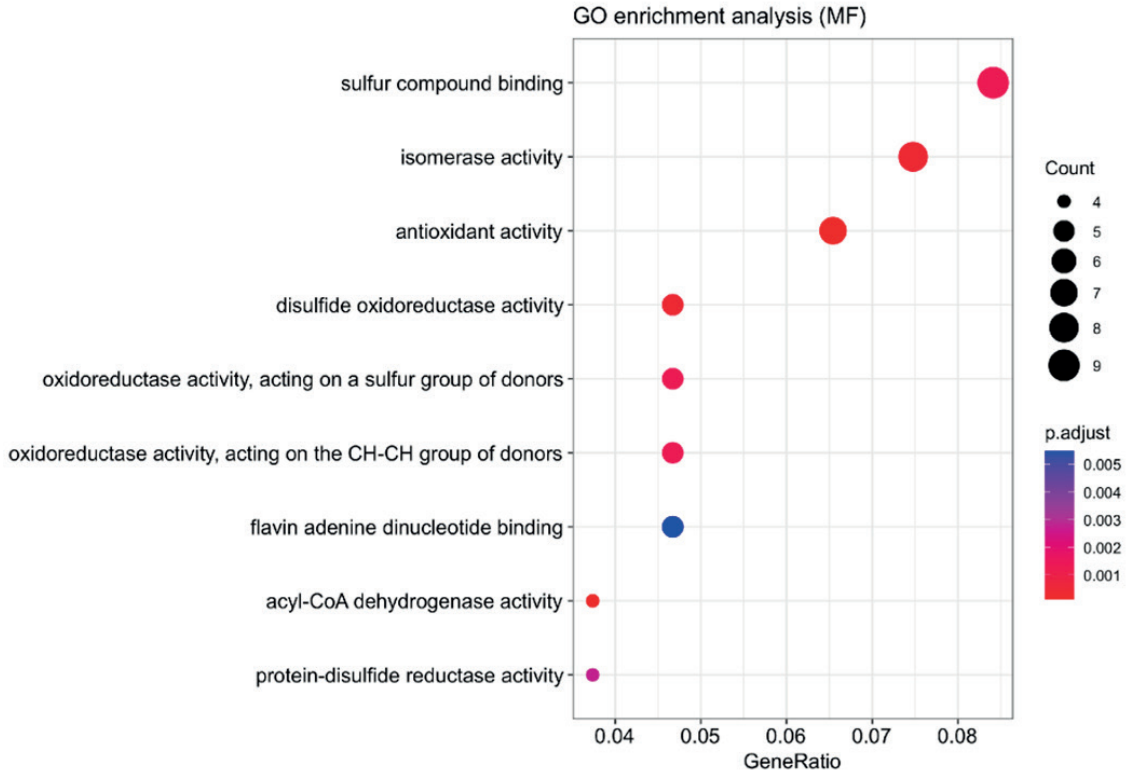

F

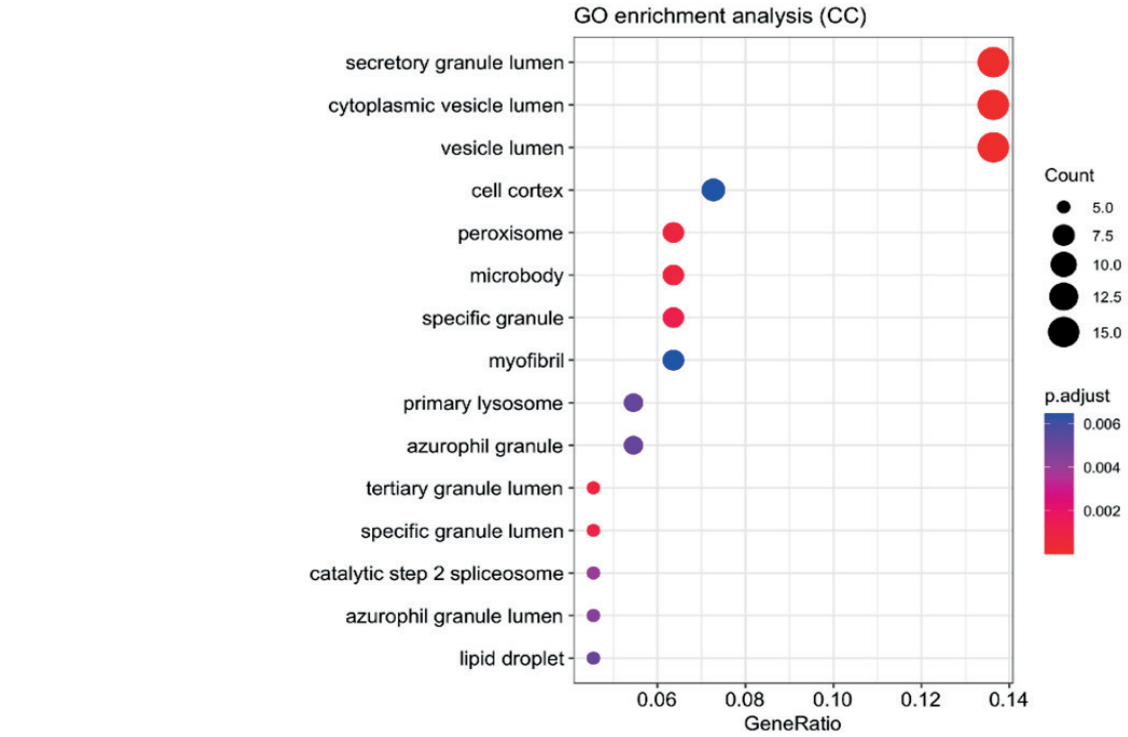

Indexed in: [Science Citation Index Expanded] [Index Medicus/MEDLINE] [Chemical Abstracts] [Scopus]

G

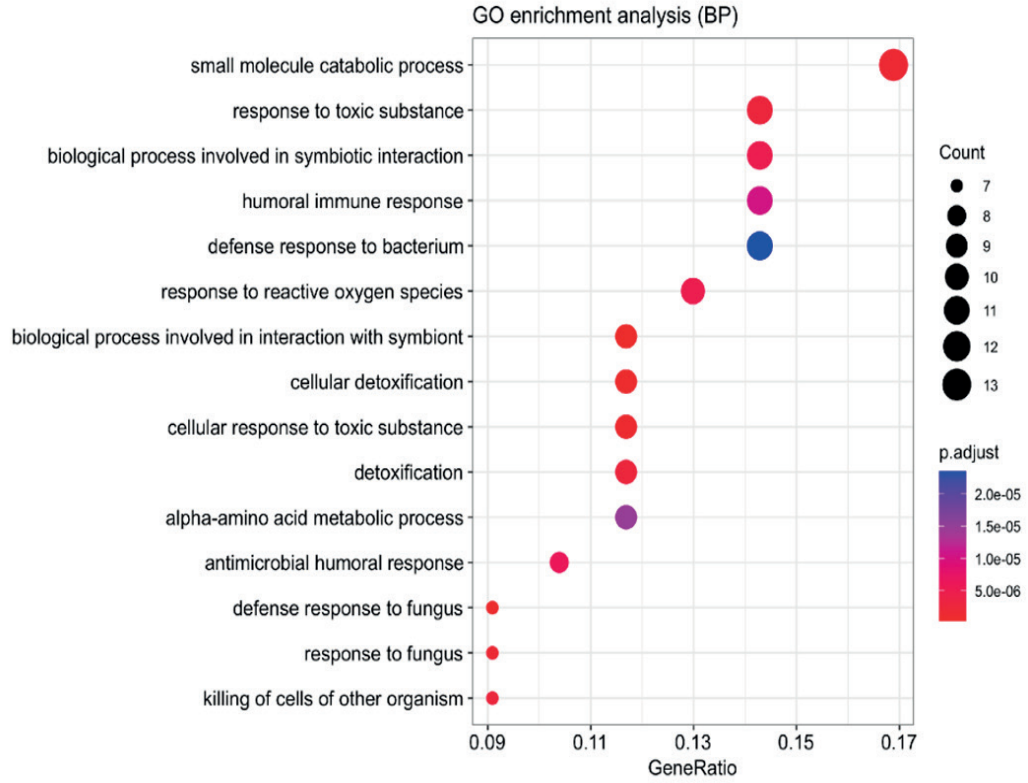

H

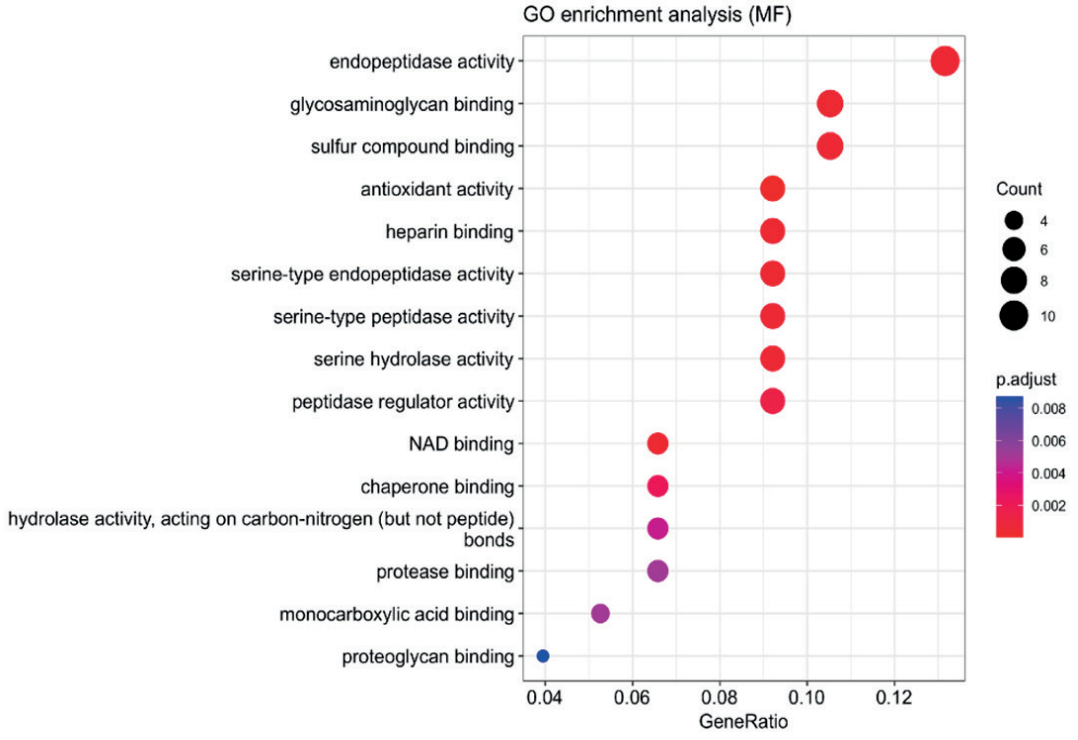

Indexed in: [Science Citation Index Expanded] [Index Medicus/MEDLINE] [Chemical Abstracts] [Scopus]

I

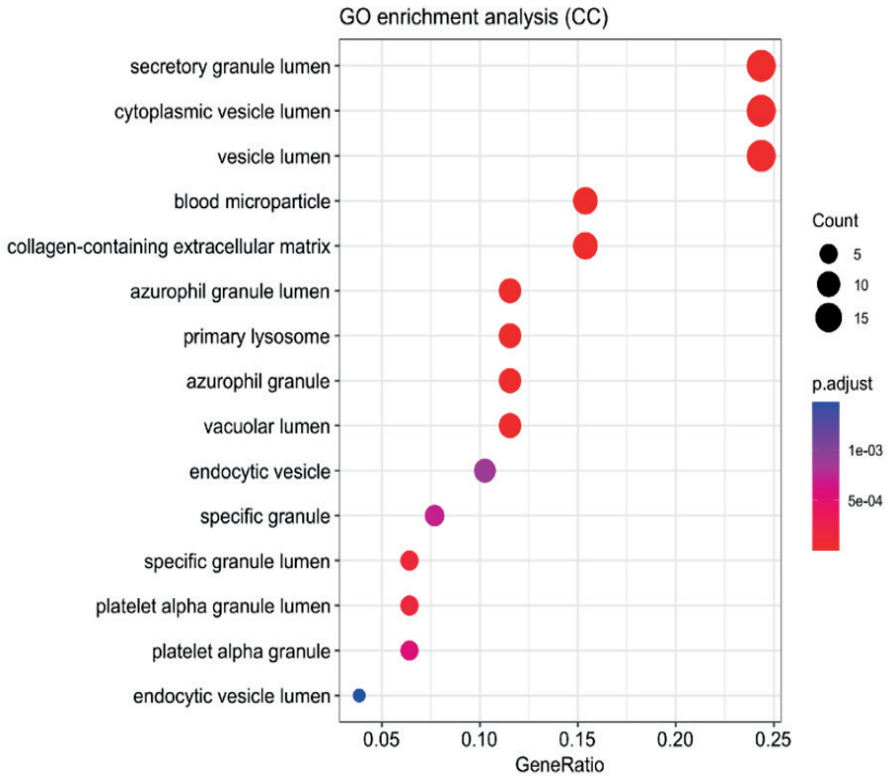

Figure 5. GO functional enrichment of PNF2, EAD2, OG groups, and Control group, respectively. (**A-C**) PNF2-Control group GO-BP, MF, CC. (**D-F**) EAD2-Control group GO-BP, MF, CC. (**G-I**) OG-Control group GO-BP, MF, CC.

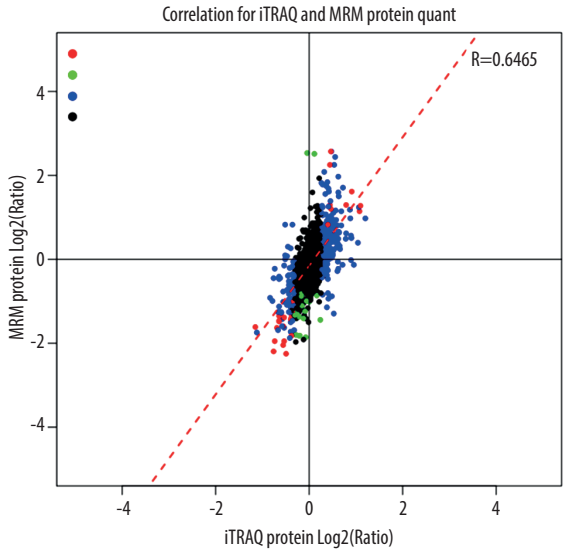

Figure 6. Technical correlation between iTRAQ and MRM quantification. The scatter plot demonstrates the quantitative consistency of the log2 fold changes for the screened proteins across the 2 independent mass spectrometry platforms, serving as a methodological validation.

Indexed in: [Science Citation Index Expanded] [Index Medicus/MEDLINE] [Chemical Abstracts] [Scopus]

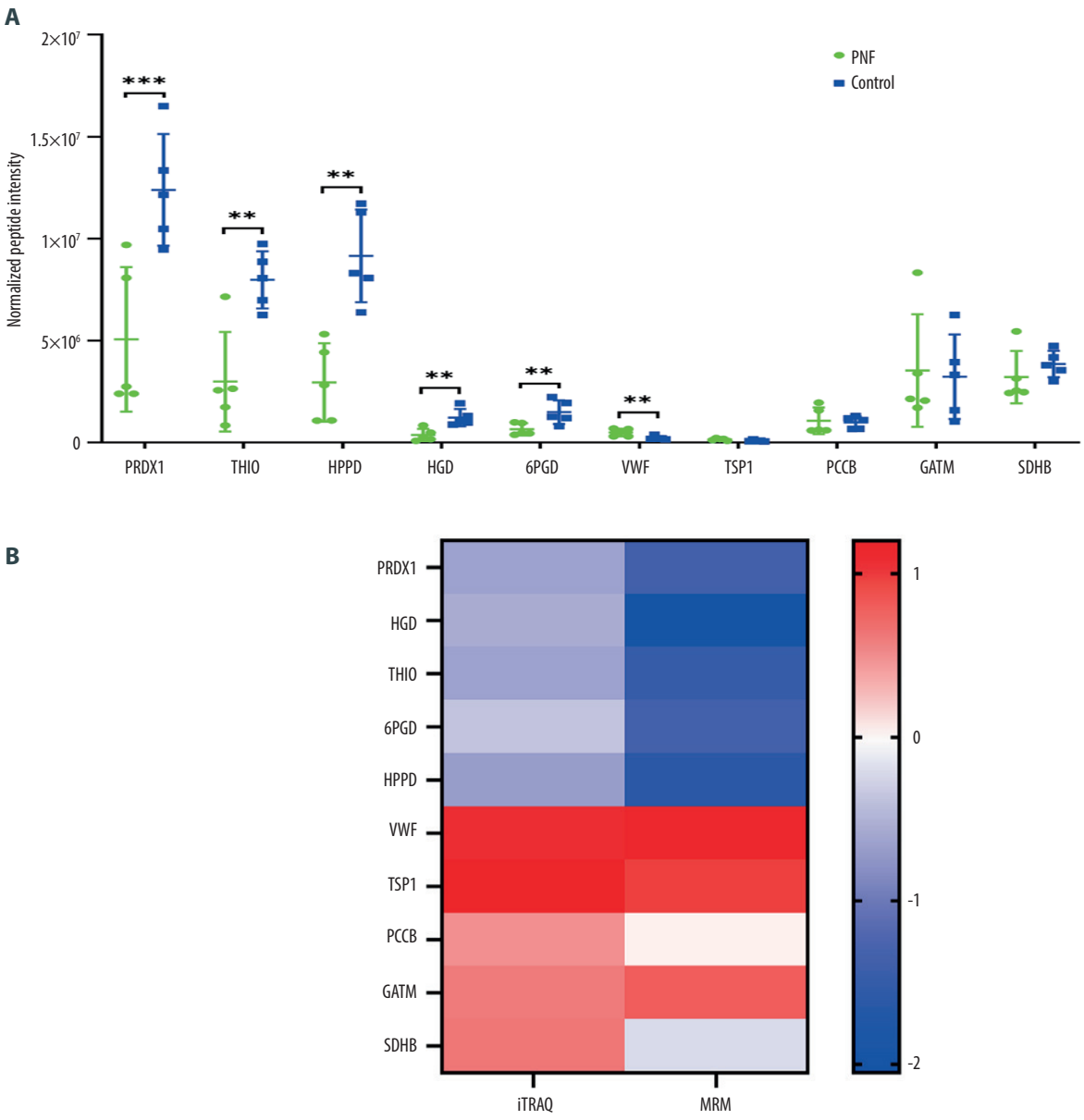

Figure 7. Verification of target proteins using MRM assay. (**A**) The different normalized peptide intensity detected by MRM assay, n=5, ** FDR <0.01, *** FDR <0.001, FDR <0.05 means a significant difference. (**B**) Heat map showing the change in abundance of differentially expressed proteins in PNF2 vs Control group, as measured using iTRAQ (**left panel**) and MRM (**right panel**).

Metabolism, Fatty Acid Degradation, and others (**Figure 4C**). These proteins were mostly associated with cell parts and organelles in cellular components, and binding and catalytic activity in molecular function, indicating their key roles in enzymatic and regulatory processes. Results of comprehensive GO enrichment analyses for each experimental group compared to the Control group are presented in **Figure 5**.

The identified DAPs were enriched in several important signaling pathways, including Metabolic Pathways, IL-17 Signaling, Ras Signaling, TNF Signaling, PPAR Signaling, and Estrogen Signaling, all of which are linked to inflammation, metabolism, and immune regulation.

PNF-Associated Proteins and Key Roles in Oxidative Stress and Energy Metabolism

To validate the candidate proteins identified through proteomic analysis, MRM was performed to quantify the differential expression of target proteins in the liver. Initially, 119 proteins

Indexed in: [Science Citation Index Expanded] [Index Medicus/MEDLINE] [Chemical Abstracts] [Scopus]

Table 4. MRM validation of differentially expressed proteins identified by iTRAQ.

Protein symbol	iTRAQ Fold change (±SD)	MRM Fold change (±SEM)	Log2 Fold change	95% CI	MRM FDR	PNF2 vs control
PRDX1	0.64±0.20	0.39±0.13	-1.36	[0.15, 0.80]	<0.001	Downregulation*
HGD	0.68±0.09	0.24±0.12	-2.06	[0.02, 0.58]	0.00134	Downregulation*
THIO	0.64±0.10	0.36±0.14	-1.47	[0.04, 0.71]	0.00143	Downregulation*
HPPD	0.62±0.22	0.32±0.10	-1.64	[0.09, 0.55]	0.00127	Downregulation*
6PGD	0.77±0.12	0.39±0.12	-1.36	[0.15, 0.72]	0.00128	Downregulation*
SDHB	1.54±0.45	0.86±0.16	-0.22	[0.44, 1.23]	0.531	Downregulation
VWF	2.11±1.07	2.21±0.57	1.14	[1.28, 3.95]	0.00206	Upregulation*
GATM	1.52±0.18	1.74±0.50	0.80	[0.40, 2.99]	0.211	Upregulation
PCCB	1.4±0.19	1.03±0.33	0.04	[0.26, 1.91]	0.933	Upregulation
TSP1	2.3±1.19	1.97±0.49	0.98	[0.65, 2.93]	0.154	Upregulation

All comparisons were performed using the *t* test (2-tailed, df=8). FDR* <0.05 means a significant difference.

were selected for MRM verification based on their differential expression in IRI. Of these, 103 proteins were suitable for MRM analysis. After further screening, 40 proteins with a high fold change and clear association with hepatic injury were chosen for final MRM validation. The MRM quantitative analysis showed a significant positive correlation with the iTRAQ results (**Figure 6**, R=0.6465), confirming the technical consistency and reliability of the proteomic data across the 2 distinct mass spectrometry platforms.

In the comparison of the 160 uniquely differentially expressed proteins in the PNF2 and Control groups, 10 proteins were selected for further MRM validation. These proteins included: PRDX1, HGD, THIO, 6PGD, HPPD, VWF, TSP1, PCCB, GATM, and SDHB. As shown in **Figure 7A**, the expression levels of PRDX1, HGD, THIO, 6PGD, and HPPD were significantly downregulated in the PNF2 group compared to the Control group. Conversely, VWF was significantly upregulated (**Figure 7A, 7B**). The remaining 4 proteins (PCCB, TSP1, GATM, and SDHB) showed no significant differences in expression between the PNF2 and Control groups after IRI (**Figure 7A, 7B**). Quantitative data, including iTRAQ fold changes, MRM fold changes, MRM log2fold change, and MRM FDR values, are provided in **Table 4**. Proteins that were verified by MRM were further grouped according to their subcellular localization and functional roles, as shown in **Table 5**. Notably, all the significantly downregulated proteins were linked to oxidative stress and energy metabolism pathways. In contrast, the significantly upregulated protein VWF is primarily involved in cell adhesion and blood coagulation, and it is generally derived from the extracellular matrix. These results suggest that the identified biomarker panel reflects the generic insult of ischemia-reperfusion and PNF-specific failure of protective mechanisms during the early reperfusion phase, thereby exhibiting stage-specific and disease-specific characteristics.

Discussion

PNF is the most severe form of liver IRI, inevitably resulting in graft failure and necessitating emergency retransplantation, which carries a remarkably high mortality rate [20-22]. The multifactorial nature of PNF – often linked to extended criteria donors (ECDs), prolonged ischemia, and severe steatosis – makes early clinical prediction highly challenging. In this study, we used a rigorous iTRAQ and MRM proteomic pipeline to identify a highly specific biomarker panel (PRDX1, HGD, THIO, 6PGD, HPPD, and VWF). Crucially, the altered expression of these 6 proteins was observed at the post-reperfusion stage (T2) in grafts that subsequently developed PNF. This underscores that our findings reflect a PNF-specific molecular collapse rather than a generalized surgical or IRI response.

Rather than simply mirroring general hepatic IRI, our proteomic data reveal that PNF is characterized by a profound failure in specific metabolic and antioxidant defenses. We observed a significant downregulation of HGD and HPPD, 2 critical enzymes in phenylalanine and tyrosine catabolism [23,24]. Because these amino acids are essential glucogenic and ketogenic energy sources, the suppression of HGD and HPPD indicates a severe disruption in energy supply during the critical early reperfusion phase. Beyond mere energy deprivation, the metabolic bottleneck caused by HGD and HPPD downregulation can lead to toxic accumulation of intermediate

Indexed in: [Science Citation Index Expanded] [Index Medicus/MEDLINE] [Chemical Abstracts] [Scopus]

Table 5. Functions and localization of the verified proteins by MRM.

Probe set ID	Protein symbol	Description	Subcellular localization	Function	PNF2 vs control
897	**PRDX1**	Peroxiredoxin-1	Cytoplasmic/ nucleus	Oxidative stress; cell proliferation; energy metabolism	Downregulation*
2272	**HGD**	Homogentisate 1,2-dioxygenase	Nucleus	Oxidative stress; metal ion binding; energy metabolism	Downregulation*
4145	**THIO**	Thioredoxin	Nucleus/ mitochondrial	Oxidative stress; cell proliferation; energy metabolism	Downregulation*
6344	**HPPD**	4-hydroxyphenylpyruvate dioxygenase	Nucleus	Oxidative stress; metal ion binding; production of no; energy metabolism	Downregulation*
5209	**6PGD**	6-phosphogluconate dehydrogenase	Cyto_pero/ nucleus	Energy metabolism	Downregulation*
4495	**SDHB**	Succinate dehydrogenase [ubiquinone] iron-sulfur subunit	Mitochondrial	Metal ion binding; energy metabolism	Downregulation
220	**VWF**	Von Willebrand factor	Extracellular	Cell adhesion; blood coagulation	Upregulation*
3492	**GATM**	Glycine amidinotransferase	Mitochondrial	Oxidative stress; energy metabolism	Upregulation
2709	**PCCB**	Propionyl-CoA carboxylase beta chain	Mitochondrial	Fatty acid metabolism	Upregulation
1847	**TSP1**	Thrombospondin-1	Nucleus/ cyto_pero mitochondrial	Oxidative stress; fatty acid metabolism; calcium ion binding; immune response; energy metabolism; cell proliferation	Upregulation

metabolites, such as maleylacetoacetate and fumarylacetoacetate [25]. These accumulated intermediates are known to be highly reactive and hepatotoxic, directly inducing hepatocellular apoptosis and further exacerbating cellular stress [26-28]. This metabolic paralysis prevents the graft from recovering basic cellular functions, directly contributing to the irreversible nature of PNF [29].

Furthermore, the significant downregulation of THIO, 6PGD, and PRDX1 highlights a catastrophic breakdown of the graft's reactive oxygen species (ROS) scavenging systems [30-32]. It is particularly noteworthy that 6PGD is a rate-limiting enzyme in the pentose phosphate pathway, which is the primary cellular source of NADPH. Because both the thioredoxin (THIO) and glutathione antioxidant systems strictly rely on NADPH to regenerate their active forms, the simultaneous drop in 6PGD and THIO represents a systemic collapse of the entire NADPH-dependent antioxidant axis, rather than just isolated enzyme failures. This specific depletion leaves the PNF graft defenseless against massive ROS bombardment from activated Kupffer cells upon reperfusion. Specifically, the loss of PRDX1, which normally modulates the microenvironment by inhibiting macrophage adhesion, likely exacerbates the unchecked inflammatory cascade unique to PNF [33,34].

In stark contrast to the downregulated protective enzymes, Von Willebrand Factor (VWF) was significantly upregulated in the PNF group. VWF is a major driver of platelet aggregation and microthrombus formation and thrombus formation is one of the key contributors to PNF [35]. Mechanistically, we hypothesize that the systemic collapse of antioxidant defenses (THIO/6PGD/PRDX1) leads to overwhelming oxidative damage to the liver sinusoidal endothelial cells. This severe endothelial injury triggers massive exocytosis of ultra-large VWF

Indexed in: [Science Citation Index Expanded] [Index Medicus/MEDLINE] [Chemical Abstracts] [Scopus]

multimers into the microcirculation. The resulting microthrombi block blood flow, abruptly worsening local hypoxia, which in turn accelerates the metabolic failure (HGD/HPPD) and generates even more ROS. The simultaneous alteration of these 6 proteins essentially maps out a lethal, self-amplifying "vicious cycle" – metabolic failure, unbuffered oxidative stress, and microvascular thrombosis – that drives the irreversibility of PNF [36,37].

Despite these promising findings, several limitations of our study must be acknowledged. First, the definition and selection of our Control group present challenges for direct clinical applicability. We used pre-perfusion biopsies from optimal organ donors to establish a pristine molecular baseline. However, clinically, ECDs inherently possess different baseline molecular profiles than optimal donors. Second, due to the relatively small sample size and the highly restrictive criteria used to define PNF, our results must be strictly interpreted as hypothesis-generating rather than definitive. While the identified 6-protein panel is highly promising and biologically consistent with PNF pathology, it currently serves as a foundation for future targeted studies.

Conclusions

Our study used an integrated iTRAQ and MRM-based proteomic approach to identify a stage-specific biomarker panel associated with PNF after LT. By focusing on the critical post-reperfusion phase, we identified 6 proteins – PRDX1, HGD, THIO, 6PGD, HPPD (downregulated), and VWF (upregulated) – that are uniquely dysregulated in PNF grafts, indicating a correlation between this biomarker panel and the occurrence of PNF. This panel holds promise for the early identification of patients at high risk of reperfusion injury following LT, who may consequently benefit from improved and individualized therapeutic strategies. Further prospective studies are required to determine whether biomarker-guided strategies can improve outcomes in LT.

Declaration of Figures' Authenticity

All figures submitted have been created by the authors who confirm that the images are original with no duplication and have not been previously published in whole or in part.

Abbreviations

LT – liver transplantation; **EAD** – early allograft dysfunction; **PNF** – primary dysfunction; **OG** – optimal graft; **IRI** – ischemia-reperfusion injury; **BMI** – body mass index; **DCD** – cardiac death donor; **ICU** – intensive care unit; **iTRAQ** – isobaric tags for relative and absolute quantitation; **MRM** – multiple reaction monitoring; **KEGG** – Kyoto Encyclopedia of Genes and Genomes; **COG** – Clusters of Orthologous Groups of Proteins; **FDR** – false discovery rate; **CV** – coefficient of variation; **SEM** – standard error of the mean; **IQR** – median with interquartile range; **MELD** – Model for End-Stage Liver Disease; **CIT** – cold ischemia time, **WIT** – warm ischemia time; **GO** – Gene Ontology; **DAPs** – differentially abundant proteins; **ECDs** – extended criteria donors; **ROS** – reactive oxygen species; **THIO** – thioredoxin; **VWF** – von Willebrand Factor.

References:

1. Lee DD, Singh A, Burns JM, et al. Early allograft dysfunction in liver transplantation with donation after cardiac death donors results in inferior survival. Liver Transplantation. 2014; 20(12):1447-53
2. De Carlis R, Di Sandro S, Lauterio A, et al. Liver grafts from donors after circulatory death on regional perfusion with extended warm ischemia compared with donors after brain death. Liver Transpl. 2018; 24(11):1523-35
3. Olthoff KM, Kulik L, Samstein B, et al. Validation of a current definition of early allograft dysfunction in liver transplant recipients and analysis of risk factors. Liver Transplantation. 2010;16(8):943-49
4. Rayar M, Sandri GBL, Cusumano C, et al. A score model for the continuous grading of early allograft dysfunction severity. Liver Transplant. 2016;22(6):859-60
5. Hartog H, Hann A, Perera MTPR. Primary nonfunction of the liver allograft. Transplantation. 2022;106(1):117-28
6. Carrier FM, Trottier H, Soucy-Proulx M, et al. Risk factors for in-hospital postoperative complications and 6-month graft survival after liver transplantation: A multicenter cohort study. Liver Transplant. 2026;32(3):400-10
7. Zhang QY, Zhang QF, Zhang DZ. The impact of steatosis on the outcome of liver transplantation: A meta-analysis. Biomed Res Int. 2019;2019:5190178
8. Cameron AM, Ghobrial RM, Yersiz H, et al. Optimal utilization of donor grafts with extended criteria: A single-center experience in over 1000 liver transplants. Ann Surg. 2006; 243(6):748-55
9. Sirivatanauksorn Y, Taweerutchana V, Limsrichamrern S, et al. Recipient and perioperative risk factors associated with liver transplant graft outcomes. Transplant Proc. 2012; 44(2):505-8
10. Brokelman W, Stel AL, Ploeg RJ. Risk factors for primary dysfunction after liver transplantation in the university of wisconsin solution era. Transplant Proc. 1999;31(5):2087-90
11. Justo I, Nutu A, García-Conde M, et al. Incidence and risk factors of primary non-function after liver transplantation using grafts from uncontrolled donors after circulatory death. Clin Transplant. 2021;35(1):e14134
12. Neves DB, Rusi MB, Diaz LGG, et al. Primary graft dysfunction of the liver: Definitions, diagnostic criteria and risk factors. Einstein (São Paulo). 2016;14(4):567-72
13. Gierej P, Radziszewski M, Figiel W, et al. Advancements in predictive tools for primary graft dysfunction in liver transplantation: A comprehensive review. J Clin Med. 2024;13(13):3762
14. Lee BT, Fiel MI, Schiano TD. Antibody-mediated rejection of the liver allograft: An update and a clinico-pathological perspective. J Hepatol. 2021;75(5):1203-16
15. Masior Ł, Grąt M. Primary nonfunction and early allograft dysfunction after liver transplantation. Digest Dis. 2022;40(6):766-76
16. Pan Q, Zhou A, Wang B, et al. Diagnostic and predictive biomarkers of acute rejection after liver transplantation. Int Jo Surg. 2025;111(6):3908-19
17. Kornasiewicz O, Bojarczuk K, Bugajski M, et al. Application of a proteomic approach to identify proteins associated with primary graft non-function after liver transplantation. Int J Mol Med. 2012;30(4):755-64
18. Wang K, Wang Y, Wang X, et al. Comparative salivary proteomics analysis of children with and without dental caries using the iTRAQ/MRM approach. J Transl Med. 2018;16(1):11

Indexed in: [Science Citation Index Expanded] [Index Medicus/MEDLINE] [Chemical Abstracts] [Scopus]

19. Máthé Z, Paul A, Molmenti EP, et al. Liver transplantation with donors over the expected lifespan in the model for end-staged liver disease era: Is mother nature punishing us?: Liver transplantation with donors over the expected lifespan. Liver Int. 2011;31(7):1054-61
20. Li J, Li RJ, Lv GY, Liu HQ. The mechanisms and strategies to protect from hepatic ischemia-reperfusion injury. Eur Rev Med Pharmacol Sci. 2015;19(11):2036-47
21. Ali JM, Davies SE, Brais RJ, et al. Analysis of ischemia/reperfusion injury in time-zero biopsies predicts liver allograft outcomes. Liver Transplant. 2015;21(4):487-99
22. Verhelst X, Geerts A, Jochmans I, et al. Glycome patterns of perfusate in livers before transplantation associate with primary nonfunction. Gastroenterology. 2018;154(5):1361-68
23. Ates I, Stuart C, Rathbone T, et al. Ex vivo gene editing and cell therapy for hereditary tyrosinemia type 1. Hepatol Commun. 2024;8(5):e0424
24. Wilson PJM, Ranganath LR, Bou-Gharios G, et al. Expression of tyrosine pathway enzymes in mice demonstrates that homogentisate 1,2-dioxygenase deficiency in the liver is responsible for homogentisic acid-derived ochronotic pigmentation. JIMD Rep. 2021;58(1):52-60
25. Bernardini G, Braconi D, Zatkova A, et al. Alkaptonuria. Nat Rev Dis Primers. 2024;10(1):16
26. Yang X, Chen SL, Lin CS, et al. Tyrosine metabolic enzyme HPD is decreased and predicts unfavorable outcomes in hepatocellular carcinoma. Pathol Res Pract. 2020;216(11):153153
27. Ascher DB, Spiga O, Sekelska M, et al. Homogentisate 1,2-dioxygenase (HGD) gene variants, their analysis and genotype–phenotype correlations in the largest cohort of patients with AKU. Eur J Hum Genet. 2019;27(6):888-902
28. Tong M, Wong TL, Zhao H, et al. Loss of tyrosine catabolic enzyme HPD promotes glutamine anaplerosis through mTOR signaling in liver cancer. Cell Rep. 2021; 36(8):109617
29. Zhang X, Zhang C, Huang H, et al. Primary nonfunction following liver transplantation: Learning of graft metabolites and building a predictive model. Clin Transl Med. 2021;11(7):e483
30. Kisucka J, Chauhan AK, Patten IS, et al. Peroxiredoxin1 prevents excessive endothelial activation and early atherosclerosis. Circ Res. 2008;103(6):598-605
31. Sun K, Eriksson SE, Tan Y, et al. Serum thioredoxin reductase levels increase in response to chemically induced acute liver injury. Biochim Biophys Acta. 2014;1840(7):2105-11
32. Aydemir D, Öztaşcı B, Barlas N, et al. Effects of butylparaben on antioxidant enzyme activities and histopathological changes in rat tissues. Arch Hig Rada Toksikol. 2019;70(4):315-24
33. Lu D, Wang W, Liu J, et al. Peroxiredoxins in inflammatory liver diseases and ischemic/reperfusion injury in liver transplantation. Food Chem Toxicol. 2018;113:83-89
34. Zhang Z, Ji Z, He J, et al. Guanine nucleotide-binding protein G(i) subunit alpha 2 exacerbates NASH progression by regulating peroxiredoxin 1-related inflammation and lipophagy. Hepatology. 2021;74(6):3110-26
35. Yoshikawa T, Nomi T, Sakai K, et al. Ischaemia–reperfusion injury with pringle's maneuver induces unusually large von willebrand factor multimers after hepatectomy. Thromb Res. 2019;183:20-27
36. Urisono Y, Sakata A, Matsui H, et al. Von willebrand factor aggravates hepatic ischemia–reperfusion injury by promoting neutrophil recruitment in mice. Thromb Haemost. 2018;47(04):700-8
37. Martins RM, Teodoro JS, Furtado E, et al. Recent insights into mitochondrial targeting strategies in liver transplantation. Int J Med Sci. 2018;15(3):248-56

Indexed in: [Science Citation Index Expanded] [Index Medicus/MEDLINE] [Chemical Abstracts] [Scopus]